A High Performance All-Polymer Symmetric Faradaic Deionization Cell

Alba Fombona-Pascual[a], Nagaraj Patil[*a], Enrique García-Quismondo [a], Nicolas Goujon[b], David Mecerreyes[b,c],

Rebeca Marcilla[a], Jesús Palma[a] and Julio J. Lado[*a]

[a]*Electrochemical Processes Unit, IMDEA Energy Institute, Avda. Ramón de la Sagra 3, 28935, Móstoles, Madrid, Spain.*

[b]*POLYMAT, University of the Basque Country UPV/EHU,Avenida Tolosa 72, Donostia-San Sebastián 20018, Spain*

[c]*IKERBASQUE Basque Foundation for Science 48013 Bilbao, Spain*

Corresponding Author(s): Julio J. Lado and Nagaraj Patil

Telephone: (+34) 91 737 11 20

E-mail: julio.lado@imdea.org / nagaraj.patil@imdea.org

ABSTRACT

Faradaic deionization (FDI) is an emerging and promising electrochemical technology for stable and efficient water desalination. Battery-type energy storage materials applied in FDI have demonstrated to achieve higher salt removal capacities than carbon-based conventional capacitive deionization (CDI) systems. However, most of the reported FDI systems are based on inorganic intercalation compounds that lack cost, safety and sustainability benefits, thereby curtailing the development of a feasible FDI cell. In this work, we introduce an all-polymer rocking chair practical FDI cell, with a symmetric system composed by a redox-active naphthalene-polyimide (named as PNDIE) buckypaper organic electrodes. First, electrochemical performance of PNDIE in 0.05 M NaCl under open-air conditions is evaluated in both three-electrode half- and symmetric FDI full-cell using typical lab-scale electrode dimensions (1.6 mg_{PNDIE}; 0.78 cm^2), revealing promising specific capacity (115 mAh g^{-1}) and excellent cycle stability for full-cell experiments (77 % capacity retention over 1000 cycles). Then, all-polymer rocking chair FDI flow cell was constructed with practical PNDIE electrodes (92.2 mg_{PNDIE}; 9.6 cm^2) that delivered large desalination capacity (155.4 mg g^{-1} at 0.01 A g^{-1}) and high salt-removal rate and productivity (3.42 mg g^{-1} min^{-1} at 0.04 A g^{-1} and 62 L h^{-1} m^{-2}, respectively). In addition, long-term stability (23 days) experiments revealed salt adsorption capacity (*SAC*) retention values over 95% after 100 cycles. The overall electrochemical and deionization performances of the reported technology is far superior than the state-of-the-art CDI and FDI techniques, making it a competitive choice for robust and sustainable “water-energy” electrochemical applications.

KEYWORDS

Faradaic deionization; Desalination; Na^+ removal; Polyimide; Electrochemical Ion Pumping; Water-Energy Nexus.

1. Introduction

The importance of ensuring the access to water and sanitation for all has been recognizing by the by the United Nations (UN) in the 6th Goal of the 2030 Agenda for Sustainable Development [1]. Additionally, the UN World Water Development Report of 2021 has estimated that over 2 billion people live in areas that are subjected to water stress and, additionally, over 45 % of the global population lack access to safely managed sanitation facilities [2]. Along with these issues, it has been found that the depletion of natural freshwater sources drives the need for replacing aging related infrastructures by new water treatment technologies. It is envisioned that these advanced treatments should face challenges such as the adaptation to climate change and the reduction of energy consumption [3,4]. As a result, many efforts have been devoted, specially, in the development of efficient and low-cost desalination systems [3]. Currently, the most popular desalination technologies are multi-stage flash distillation (MSF) and reverse osmosis (RO) [5–7]. However, both treatments have a relatively high energy consumption (from 3-5 kWh m^{-3} in the case of RO to 10-16 kWh m^{-3} in the case of MSF) due to the use of either high temperatures or pressures applied in the desalination process [5,6], [8].

To overcome these limitations, electrochemical technologies have recently attracted the attention of the scientific community [9]–[14]. Carbon electrodes have been employed in a process named capacitive deionization (CDI) for ion separation, whose working mechanism is driven by the formation an electrical double layer (EDL). CDI is an energy-efficient and environmentally friendly technology [14], [15], [16] based on the application of low voltages (usually below 1.5 V). In this fashion, CDI avoids the drawbacks of using an energy-intensive thermal process or operating under high-pressure conditions, reducing the energy consumption per volume of fresh water produced from brackish water (0.2-1.0 kWh m^{-3}) [17–19]. Nevertheless, along with the adsorption of the counterions during the charging process, co-ions are released simultaneously, resulting in a significant charge losses [3,16]. To address this problem, ion exchange membranes (IEM) have been placed alongside the electrodes, configuring membrane CDI technology (MCDI) [16,20]. Despite the use of costly IEM, the ion removal capacity of these deionization systems is not sufficient yet for desalting high-concentration saline water [5,21] being its application limited to brackish water (1-5 g L^{-1}) desalination.

As an alternative, in 2012 M. Pasta *et al.* introduced “A Desalination Battery”-an innovative system in which the electrode was made up of an active material that was able to store the ions within its particles/layers by either intercalation and/or faradic reactions [11]. Here onwards term “faradaic deionization (FDI)” is used to describe this and related technologies. Later, Lee *et al.* proposed a hybrid capacitive deionization (HCDI) system that combines EDL-based and faradaic materials as cell’s electrodes [11], [21]. Faradaic materials, typically used in batteries for energy storage, are able to intercalate selectively certain ions in the bulk as a result of a redox reaction, which contrasts with surface confined reactions experienced in capacitive materials [15,22,23]. Consequently, faradaic materials present large charge storage capacity (and hence high specific capacity) and high ion selectivity that concurrently lead to a high desalination (or cation recovery) capacity compared to the capacitive electrodes [5,15],[24]. Additionally, since only cations or anions will be stored in the bulk of intercalation materials due to their intrinsic redox-active mechanism, they show less co-ion expulsion than the conventional carbon electrodes [5]. In this context, many faradaic electrodes, mostly based on inorganic materials with cation-storage capability such as metal oxides (sodium manganese oxide), metal phosphates (NASICON), MXenes and Prussian blue analogues, have been reported for HCDI and FDI [5,16,17,23–32].

Lately, the development of redox-active organic materials as faradaic electrodes for more sustainable batteries technologies have been gaining renowned interest within the battery research community [33–35]. This is mainly due to their inherent features such as flexibility, easy processability, recyclability, biodegradability, the ability to be 2D or 3D printed, and the perspective to prepare them from renewable resources. Polymers are promising candidates to substitute inorganic active materials in battery electrodes because of their low specific weight, good mechanical and thermal stability, safety and sustainability aspects. Particularly, the family of carbonyl compounds (e.g., imides, quinones, etc.) is of special interest due to their high reactivity, fast kinetics, high capacity and wide structural design diversity [30,36]. The redox mechanism of carbonyl functionalities implies a reversible one-electron reduction reaction to form a radical mono-anion (enolization) accompanied by capture of an electroneutralizing cation (see **Scheme 1a** for the representative redox mechanism of a typical imide polymer in Na^+ electrolyte). Thus, this process can be extended to more electrons by expanding the conjugated structure [30,37].

Among the different carbonyl polymers, polyimides (PI) have been successfully applied as high performance organic electrodes in numerous battery technologies, including but not limited to monovalent (e.g., Li^+) and multivalent (e.g., Mg^{+2}, Al^{+3}) batteries operating in organic electrolytes [4,30]. Lately, their applicability as polymer anode for aqueous batteries with a range of charge carriers (Li^+, Na^+, Mg^{+2}, Ca^{+2}, etc.) also been realized [38–41]. Despite the impressive amount of works on the use of polymer electrodes for batteries, to the best of our knowledge, we found a sole example of redox polymer, specifically, PI, applied as polymer cathode in combination with a EDL-based electrode in a HCDI system [37,42]. However, this PI-HCDI system exhibited limited performance in terms of low specific capacity (~60 mAh g^{-1}), poor coulombic efficiency (~70 %) and moderate sodium uptake capacity (54.2 mg g^{-1}). Albeit this exciting advancement of polymer-based HCDI, there is still enormous room to improve the performance of the underlying HCDI systems. In this regard, it is also worth mentioning here that, beyond the reported PI-HCDI technology, the implementation of all-polymer FDI for ion capture technologies has not been accomplished to date.

Based on the acquired knowledge from organic batteries by our group and the specific working requirements for the efficient FDI namely, i) low electrolyte concentration (below 0.05 M) and ii) open-air atmosphere, an innovative polyimide-based symmetric FDI is proposed here. Our approach relies on the synergistic combination of smart redox polymer selection i.e., poly[N,N′-(ethane-1,2-diyl)-1,4,5,8-naphthalenetetracarboxiimide] (PNDIE) and refining it into an advanced buckypaper electrode architecture to meet the aforementioned FDI criteria. Notably, PNDIE has been proven to exhibit a stable electrochemical performance in O_2-saturated aqueous electrolytes [37]. Additionally, carbon nanotube-reinforced PNDIE buckypaper is anticipated to furnish superior electrochemical performance due to its intrinsic enhanced electron/ion transport even with high polymer content and high mass loading organic electrodes as already demonstrated in batteries [43–45] that are also specific working requirements of a practical FDI system.

In this work, the electrochemical and deionization performances of the PNDIE electrodes in a standard three electrode half-cell, symmetric coin cell, and a rocking-chair FDI full-cell configurations were quantified by systematically operating it under various operational conditions and comparing it with the state-of-the-art to scrutinize our results. The all-polymer PNDIE symmetric coin cell with lab-scale electrodes (~1.6 mg; 0.78 cm^2) demonstrated high specific capacity (~110 mAh g^{-1}), good coulombic efficiency (~100%) and excellent cycle stability (77 % capacity retention over 1000 cycles) in 0.05 M NaCl solution. Inspired by this superior electrochemical performance, a novel all-polymer FDI cell with larger electrodes (92.2 mg; 9.6 cm^2) was constructed by coupling a reduced PNDIE anode and an oxidized PNDIE cathode with an anion-exchange membrane. The constructed FDI cell exhibited a high salt removal capacity of 155.4 mg g^{-1} in 0.05 M NaCl solution working at constant current (CC) of 0.01 A g^{-1} and a rate adsorption capacity of almost 3.42 mg g^{-1} min^{-1} working at CC of 0.04 A g^{-1}, leading to a productivity of 62 L h^{-1} m^{-2}. These impressive values outperformed most of the previous CDI/HCDI/FDI results reported in the literature.

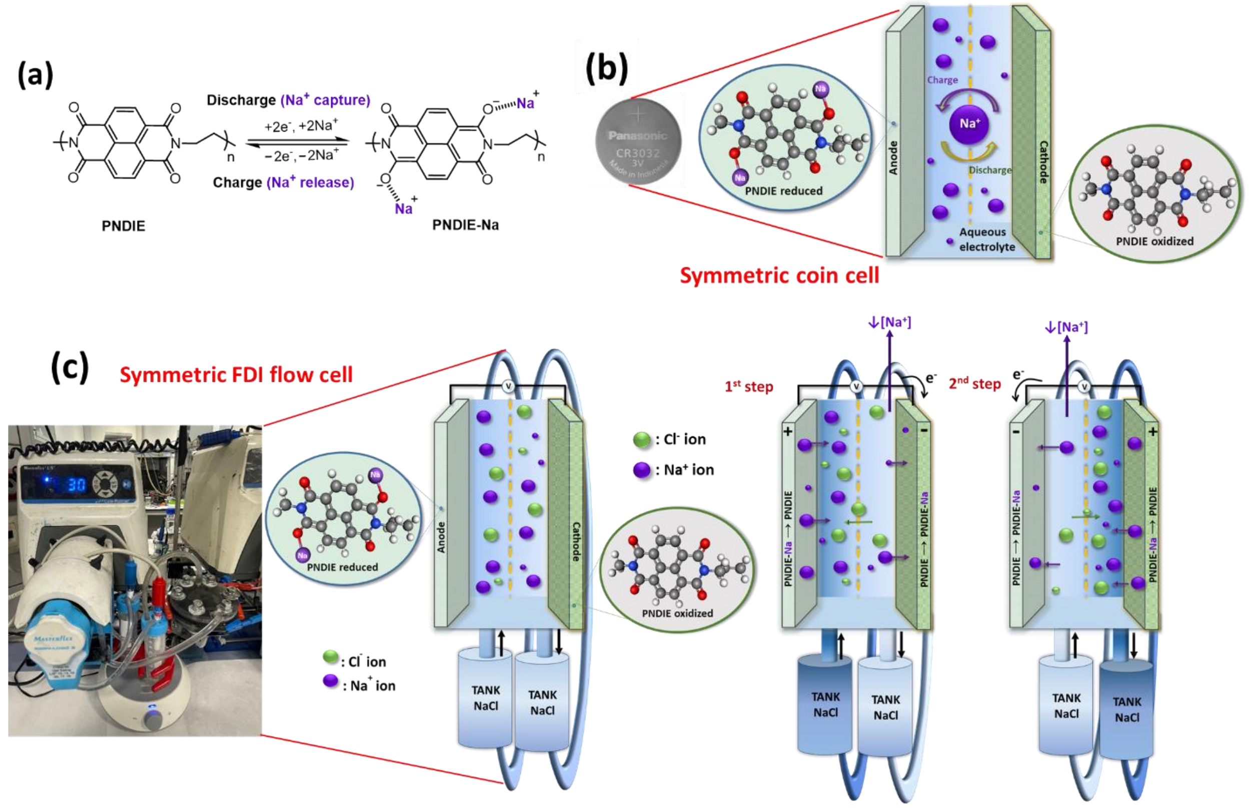

Scheme 1. Design principles of faradaic deionization using PNDIE. (a) Electrochemical redox mechanism in Na^+ aqueous electrolyte, (b) working mechanism of PNDIE symmetric coin-type and flow-type (c) full cells.

2. Experimental section

2.1 Materials and Methods

Reduced graphene oxide (RGO; Nanografi), single-walled carbon nanotubes (SWCNT; Nanografi), polyvinylidene fluoride (PVDF; Sigma Aldrich), 1-methyl-2-pyrrolidinone (NMP; ≥99 %, Sigma Aldrich), carbon nanotubes fiber fabrics current collector (Tortech Nano fibers Ltd., Israel), NaCl (≥99 %, Sigma Aldrich) were used as received. The redox polymer, 1,4,5,8-naphthalenetetracarboxylic dianhydride (NTCDA)-derived polyimide (PNDIE) was synthesized by a polycondensation reaction between NTCDA and ethylenediamine as described previously [46].

2.2 Electrode Preparation

The self-standing, binder- and metal current collector-free buckypaper electrodes were prepared following the modified procedure previously reported by us [45]. The composition of the electrode was fixed to 70:15:15 wt% (PNDIE:rGO:SWCNTs). In brief, for the FDI electrochemical cell, first, 22.5 mg of SWCNTs were dispersed in 20 mL solution of *iso*-propanol (IPA)/ *N*-methyl-2-pyrrolidone (NMP) (1/1 v/v) through a tip sonicator for 10 min at 0.75 cycles and 100 % of amplitude (ultrasonic processor UP400S, 400 W, 24 kHz). Then, after carefully grinding 22.5 mg of rGO with 105.0 mg of PNDIE, those were added to the SWCNTs dispersion and then sonicated again at 0.5 cycles and 50 % of amplitude for another 10 min. After, this dispersion was immersed in a bath sonicator (Branson 2510, 100 W, 42 kHz) for 2 h, then stirred overnight to prepare the electrode ink. The suspension was filtered through a Nylon membrane filter (47 mm diameter, pore size 0.45 µm) with the help of vacuum, followed by thorough rinsing with IPA to remove loosely bound polymer. The buckypaper was carefully peeled off from the filter, dried overnight at 70 °C under vacuum, and directly used as the electrode with an average diameter and mass loading 35 mm and 9.6 mg cm^{-2} of PNDIE, respectively. For three-electrode and coin cell studies, PNDIE buckypaper electrodes with lower mass loading of around 2.0 mg cm^{-2} were also prepared. Also for comparison, a conventional electrode with PNDIE mass loading around 1.6 mg cm^{-2} by a classical slurry-casting approach using the doctor-blade technique was fabricated as well.

2.3 Electrochemical Cell

2.3.1 Three Electrode cell

Circular discs of 10 mm diameter were cut from the buckypaper with a PNDIE mass loading of ~2.0 mg cm^{-2}. A standard flooded three-electrode electrochemical cell was assembled using PNDIE as the working electrode, platinum mesh as the counter electrode, and Ag/AgCl (3 M NaCl) as the reference electrode, respectively. NaCl-based aqueous electrolytes of different molar concentrations (i.e., 0.05, 0.10, 1.00 M) were used in these characterizations.

2.3.2 Symmetric coin cell

First, circular disc (10 mm diameter, 1.6 mg cm^{-2}) of PNDIE /SWCNTs/rGO was reduced in a three-electrode cell to PNDIE-Na. Then, PNDIE||PNDIE-Na full-cells were assembled using the reduced PNDIE /SWCNTs/rGO as the cathode, pristine PNDIE-Na:rGO:SWCNTs as the anode and a porous Whatman® glass microfiber filter (Grade GF/B) soaked with ~200 µL of 0.05 M NaCl as the aqueous electrolyte in CR2032 coin cells.

2.3.3 Symmetric FDI flow cell

We have chosen the symmetric flow cell configuration to evaluate PNDIE's FDI performance in which the same redox couple is present in both electrodes (e.g., OX + e$^-$ → RED and RED → OX +e$^-$), allowing us the use of low voltages to separate salts efficiently and continuously [47]. First, a circular disc (35 mm diameter, 9.6 mg cm^{-2}) of PNDIE buckypaper was reduced in a three-electrode cell to PNDIE-Na performing a discharge and charge process at 0.2 A g^{-1} to -1.0 V and 0.1 V, respectively, followed by a discharge process at 0.05 A g^{-1} until -1.1 V (**Fig. S1**). As shown in **Fig. S2a**, the flow cell consisted of two external cases fabricated via 3D printing, 4 Viton gaskets, and two expanded graphite current collectors with specific shapes catted with a silhouette plotter (CAMEO 4) and an anion exchange membrane (AEM, Fumapem FAA-3-30). Externally, each side of the cases was connected to two Nalgene PVC Tubing (1/16Wall, Thermo Scientific), from which the electrolyte was pumped flow through the device with a Masterflex® L/S® peristaltic pump with two heads at 30 mL min^{-1} (**Fig. S2b**).

2.4 Physico-chemical Characterization

Field-emission scanning electron microscopy (FE-SEM) was used to investigate the microstructure of the buckypaper electrodes. SEM images of the samples were collected using a JEOL JSM-7900F Prime at an acceleration voltage of 15 kV.

Ion chromatography (IC) was employed to analyze the amount of Na^+ and Cl^- ions removed during the electrochemical process in the symmetric FDI flow cell. When the experiments were reaching the selected voltage limit, samples were collected from each side of the cell. Those samples were then filtered through microfilters of 0.2 µm, diluted in a 1:10 ratio with MilliQ water, and analyzed using a 930 Compact IC Flex chromatographer. The separation column for anions was a Metrosep A SUPP 5, while for cations a Metrosep C 6-250/4.0. The effluent conductivity of each tank was measured using a flow-type conductivity meter sensION MM374, HACH.

2.5 Electrochemical Characterization

The electrochemical performance of individual electrodes in 3-electrode configuration and symmetric coin cells was investigated by cycling voltammetry (CV) and galvanostatic charge–discharge (GCD) experiments using a Biologic VMP3 multichannel Potentiostat/Galvanostat (Biologic SP-150). The CV and GCD profiles of PNDIE were obtained with PNDIE:rGO:SWCNT buckypaper (70:15:15 wt%), Ag/AgCl (3 M NaCl) and platinum mesh as the working, reference and counter electrodes, respectively, in different concentrations of NaCl (0.05, 0.10, and 1.00 M) as aqueous electrolyte. Then, the electrochemical behavior of the full cells in the coin-type device was tested by GCD experiments with a BTS4000-5V10mA Battery Testing System (CT-4008T), using different voltage windows and different current densities. As a commonly used procedure for polymer-based organic batteries, the specific capacities and current rates (C-rates) were normalized with respect to the mass of PNDIE in the buckypaper electrode.

All the electrochemical and Na^+ capture experiments were performed under open-air conditions without removing dissolved oxygen from the electrolyte solution unless specified otherwise.

2.6 Deionization Experiments

The deionization performance of the symmetric cell was examined in a novel Rocking Chair Deionization (RCD) module. As shown in **Fig. S2b** with two tanks containing 30 mL NaCl aqueous electrolyte from which the solution was pumped through the cell at 30 mL min^{-1} flow rate in a recirculation mode. To investigate the treatment performance of various operating conditions in the system, different voltage windows, different electrolyte concentrations, and current densities were studied. The voltage windows were studied in 0.05 M NaCl in the range of ± 0.7 V, ± 1.0 V, and ± 1.2 V at 0.01 A g^{-1}. Then, in the latest voltage range and with the same electrolyte concentration, different current densities were applied (0.01, 0.02, and 0.04 A g^{-1}). Finally, the concentration of the electrolyte was varied from 0.01 M to 0.03 M and 0.05 M NaCl at a flow rate of 30 mL min^{-1}.

The ion removal tests were generally initiated from the positive electrode (PNDIE-Na), in which disinsertion was achieved by applying constant current using the Biologic VMP3 multichannel. After that, the ions were captured by applying a negative constant current. During the test, the effluent ionic conductivity of each tank was measured with the flow-type conductivity meter. The accumulated ion removal capacity was then expressed as the deionized NaCl mass in one tank per half-weight of the PNDIE electrodes during the ion removal step. The captured Na$^+$ was calculated from the concentration change in the effluent measured by the conductivity meter. Additionally, the amount of Na$^+$ and Cl$^-$ ions removed during the electrochemical process was analyzed via IC.

2.7 Performance Metrics

Different figures of merit were defined to assess the performance of the desalination system:

The *salt adsorption capacity* (*SAC*, in mg g^{-1}), is expressed in terms of the amount of NaCl removed (mg NaCl) in one tank per mass of active material (g PNDIE) in one electrode when the performance reaches its equilibrium [46,48]. Then, it is calculated in Eq.1:

$$SAC = \frac{m_{NaCl\,removed}}{m_{active\,material}} \quad \textit{Equation 1}$$

The *average salt adsorption rate* (*ASAR*, in mg g^{-1} min^{-1}), calculated in Eq. 2, indicates the kinetics of desalination and is defined as the accumulated mass of deionized sodium chloride ions per total electrode mass divided by the discharge operation time (t_{DCH}, min) [21,49], and is calculated as:

$$ASAR = \frac{SAC}{t_{DCH}} \qquad \textit{Equation 2}$$

The *charge efficiency* (Λ, %, Eq. 3) quantifies the ratio of moles of salt removed from the feed (n) to amount of charge transferred between the electrodes (Q, C) during discharging [50]. F represents the Faraday constant (96485 C mol^{-1}).

$$\Lambda = \frac{nF100}{Q} \qquad \textit{Equation 3}$$

The *volumetric energy consumption* (E_V, in kWh m^{-3}) and the *molar energy consumption* (E_M, in kWh mol^{-1}) are defined in Eq. 4 and Eq. 5 as the energy needed for one half-cycle (E_c, in kWh) normalized, by the volume treated in half-cycle (V, m^3), that corresponds to the volume of one tank (30 mL), and the moles of salt removed (n) [51].

$$E_V = \frac{E_c}{V} \qquad \textit{Equation 4}$$

$$E_M = \frac{E_c}{n} \qquad \textit{Equation 5}$$

The *throughput productivity* (P, in L h^{-1} m^{-2}) is defined in Eq. 6 as the volume of treated water (V, L) normalize by the time of half-cycle (t_{DCH}, min) and the area of the electrode (A, m^2) [51].

$$P = \frac{V}{A\, t_{DCH}} \qquad \textit{Equation 6}$$

The *coulombic efficiency* (CE, in %) quantifies the ratio of electrical charge delivered during the discharge (Q_{DCH}) process to charge applied to the cell during charging (Q_{CH}) [50]. CE is defined in Eq. 7:

$$CE = \frac{Q_{DCH}}{Q_{CH}} \qquad \textit{Equation 7}$$

3. Results and discussion

3.1 Morphological characterization of the PNDIE electrode

As it was previously mentioned, the redox polymer (PNDIE) was combined with reduced graphene oxide (rGO) and single-walled carbon nanotubes (SWCNTs) through the sonication, stirring, and vacuum-assisted filtration (see Experimental Section 2.2 for the electrode preparation) to obtain a self-standing, flexible carbon mat electrode, called buckypaper. The well-known π–π interactions between rGO and/or SWCNTs and aromatic structured PNDIE (schematically represented in **Fig. S3)** were exploited to fabricate the binder- and current collector-free electrodes. **Fig. S4** shows the morphology of the PNDIE-supported buckypaper electrode by field-emission scanning electron microscopy analysis. PNDIE in the 3D randomly woven SWCNTs mat presents uniform nano-sized particulate structures, which could endow it with superior electrochemical performance due to the good ion/electron diffusion and mechanical flexibility.

This buckypaper electrode architecture has several advantages including that there is no need for an external binder, which opens the possibility to prepare high mass loading electrodes (9.6 mg cm^{-2}) and that this configuration exhibits superior rate capability, etc. [45,52]. Moreover, we emphasize in this work the suitability of adopting the buckypaper electrode architecture for the targeted application that demands efficient operability in challenging low electrolyte concentrations (below 0.05 M NaCl). The impact of using buckypaper instead of the conventional slurry-casted electrode (composed of the active material, conductive additive, and binder) will be further discussed when evaluating the electrochemical performance.

3.2 Electrochemical characterization of PNDIE

The electrochemical performance of PNDIE were studied in three different devices, i.e., i) three-electrode flooded cell, ii) two-electrode symmetric coin cell, and iii) full symmetric flow cell. In the first two device configurations, the electrolyte was in a typical static mode, while the latter device operated in a flow mode.

3.2.1 Electrochemistry of PNDIE in a three-electrode cell

The CV curves of PNDIE electrode in 1.00 M, 0.10 M, and 0.05 M NaCl solutions at 0.5 mV s^{-1}, 1.0 mV s^{-1}, and 2.0 mV s^{-1} (from 0.1 to -1.1 V *vs.* Ag/AgCl) in a three-electrode system are displayed in **Fig. S5**. As it can be observed in those figures as well as **Fig. 1a**, each CV curve exhibits two pairs of redox peaks, over -0.8 V and -0.3 V that correspond to the two-step electrochemical redox mechanism of PNDIE. That mechanism involves the reversible conversion of redox-active carbonyl groups in the imide functionality of PNDIE via enolation/carbonylation reactions followed by insertion and de-insertion of Na^+ ions during reduction/oxidation reactions, respectively, (following **Scheme 1a**) [53]. This electrochemical behavior is a clear indication of a high charge-storage capacity that is highly beneficial for electrochemical desalination applications. It is important to notice that the reduction and the oxidation peaks in the CV curves slowly shift towards the left and right, respectively, with the decrease of the electrolyte concentration indicating that the redox activity of the polyimide is weakened [37]. However, the area under the curve that represents the capacity was almost maintained with the decrease in the concentration, indicating a similar capacity of ion storing, and presumably a significant desalination capacity in these conditions. Additionally, from the potential peak position obtained at 0.5 and 2.0 mV s^{-1} scan rates and the NaCl concentration correlation (**Fig. 1b**), the linear trend confirms that the redox mechanism follows the Nernst behavior with the insertion and de-insertion of Na^+ ions [54,55].

The redox kinetics of PNDIE electrode were also investigated based on the results displayed in **Fig. 1c** using Eq. 8, where i_p is the peak current (mA), v is the scan rate (mV s^{-1}), and a and b are adjustable parameters.

$$i_p = av^b \qquad \textit{Equation 8}$$

The calculation of the b value provides relevant kinetics information. It is defined that when the value of b is close to 0.5, it normally suggests that the reactions are diffusion-limited, while a value of 1.0 indicates a fast capacitor-like charge-storage mechanism [37]. Therefore, the most pronounced reduction peak around -0.5 V vs. Ag/AgCl was taken as fitting subject to plot the log i_p vs log v (**Fig. 1c**). The b-value ranges from 0.3 to 0.5 and to 0.8 with the increment of NaCl concentration from 0.05 to 0.1 and to 1 M suggesting that PNDIE exhibits a pseudocapacitive characteristic when more ions are present in solution (ca. 1 M; as in typical battery electrolytes). On the other hand, diffusion process becomes dominant at low NaCl concentrations (e.g., 0.1 and 0.05 M; a real world brackish water desalination system works under low electrolyte concentration condition that is challenging for an organic faradaic material), thereby retarding the redox kinetics as demonstrated in the next paragraphs.

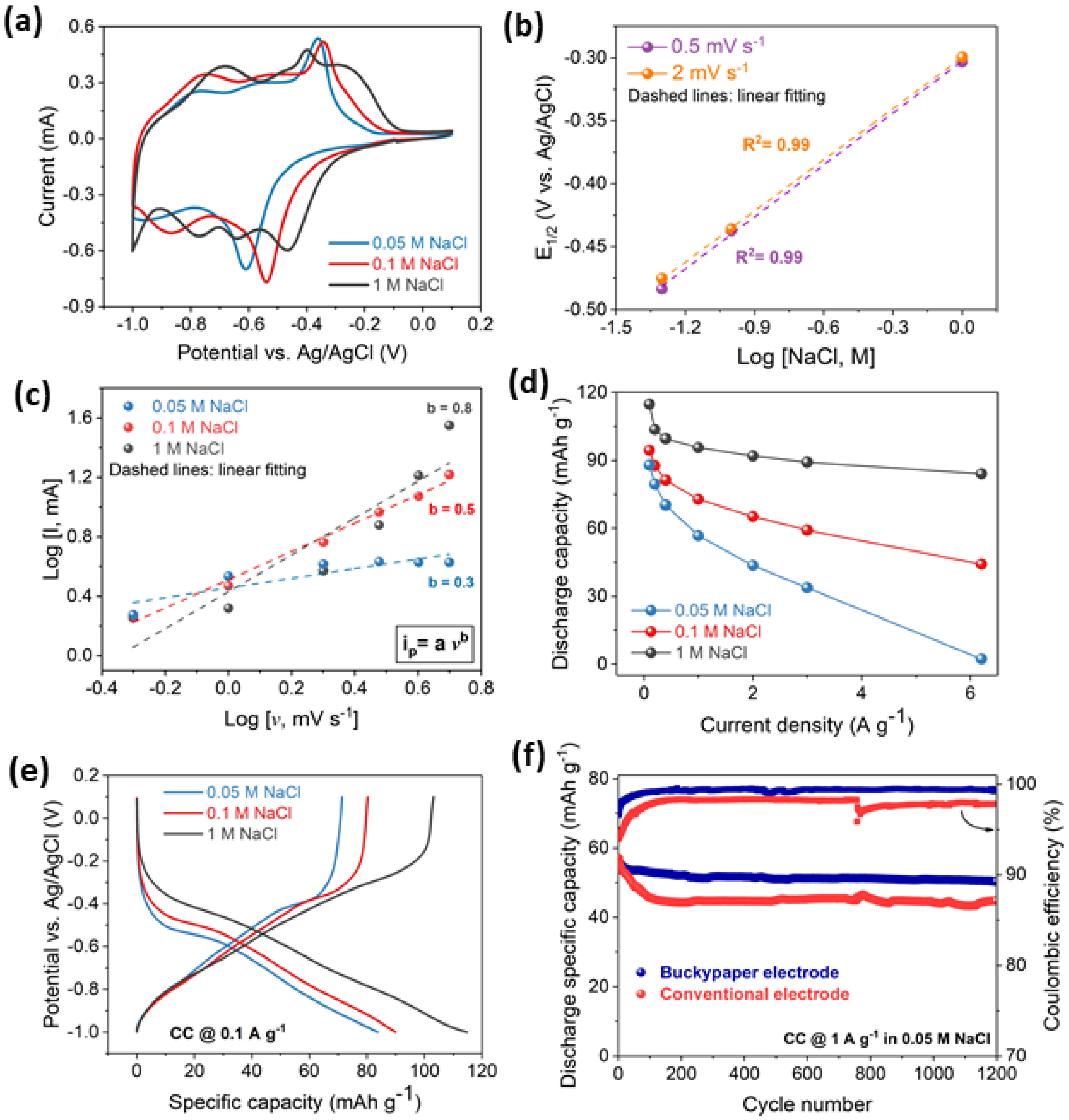

Fig. 1. PNDIE electrochemistry in a standard three-electrode cell at different NaCl aqueous electrolyte concentrations. (a) Cyclic voltammetry curves at 0.5 mV s^{-1}, (b) correlation between $E_{1/2}$ of the representative first redox couple and concentration of NaCl, and (c) power law analysis of the representative first reduction peak in the scan rate range of 0.5–2.0 mV s^{-1}. (d) Discharge capacity vs. the current density at different electrolyte concentrations, (e) the representative GCD profiles at 0.1 A g^{-1} at different electrolyte concentrations, and (f) comparison of the cycling stability at 1.0 A g^{-1} in 0.05 M NaCl of the buckypaper and the conventional slurry-casted electrode.

The GCD cycling experiments performed at different current densities using several NaCl electrolyte concentrations are shown in **Fig. S6**. Briefly, the results are quite consistent with the CV studies showing that PNDIE reached higher specific capacity values at higher electrolyte concentrations and lower current densities.

Rate capability is an important performance indicator that needs to be considered, especially when organic electrode materials are used since they suffered from slow reaction kinetics, particularly, at low electrolyte concentrations. As can be seen from **Fig. 1d**, higher current densities resulted in larger overpotential (**Fig. S6a, b and c**) rendering lower capacity values that are amplified at lower electrolyte concentrations. Additionally, as it was expected, PNDIE showed much better rate capability in the most concentrated solution (i.e., 1.0 M NaCl) compared to the diluted ones, with a capacity retention of 70 % even though the current rate increases more than 100 times (**Fig. S6d**). Moreover, when comparing the results at different electrolyte concentrations (**Fig. 1e**) only a small decrease of 29 % in the capacity (from 114.8 to 83.8 mAh g^{-1}) was observed when the NaCl concentration reduced from 1.0 to 0.05 M at 0.1 A g^{-1}. This result allows us to be moderately optimistic about the potential desalination performance of PNDIE at brackish water concentrations.

Practical water treatment can hardly afford a degassing process to avoid parasitic reactions, being open-air conditions the more common situation as long as reasonable electrochemical performance is obtained. Therefore, to check the electrochemical stability of PNDIE under an open-air environment, a cycling test at 1 A g^{-1} in 0.05 M NaCl solution was performed (**Fig. S7**). **Fig. 1f** shows that an exceptional specific capacity was maintained in the buckypaper electrode (scattered values in blue), achieving a stable capacity of 50 mAh g^{-1} after 1200 cycles. **Fig. S7a** shows a reduction of capacity from 59 to 55 mAh g^{-1} occurred just after 10 cycles, while only a small capacity decay of 15 % was observed in the subsequent 1200 cycles. Based on this, it was considered that the synthesized PNDIE buckypaper electrode demonstrated a robust performance in open-air conditions. Furthermore, a comparison between the new buckypaper PNDIE electrode configuration and the conventional slurry-casted electrode was established in terms of cycling stability revealing that the buckypaper electrode retained higher capacity (ca. 85 vs 65%) and also attained better coulombic efficiency (ca. average CE of 99 vs 97%) than the conventional electrode under similar conditions (**Fig. 1f**). It is reported that dissolved oxygen could chemically oxidize the reduced polyimide leading poor coulombic efficiencies, but without negatively affecting the chemical stability of the polymer, and thus cyclability[37][56]. This was also the case in ours and aforementioned previous studies. Of note, it should be also highlighted that the buckypaper approach enabled the preparation of much higher mass-loading electrodes than the ones produced using a conventional doctor-blade methodology (electrode cracking and delamination were observed when testing the preparation of high mass-loading electrodes).

3.2.2 Electrochemistry of PNDIE in a symmetric coin cell configuration.

The electrochemical properties of a two-electrode coin cell composed by the oxidized and reduced form of the PNDIE were analyzed. The selection of this configuration, well accepted in the battery industry [57], is supported by the idea of checking the behavior of the symmetric configuration in a static hermetically sealed system.

Initially, an analysis to evaluate the specific capacity of the PNDIE when setting different voltage windows was carried out using 0.05 M NaCl electrolyte solution. The results shown in **Fig. 2a** indicate that, as expected, larger voltage windows led to higher specific capacity values. Thus, a significant increase in the capacity was noticed when the voltage window increased beyond ± 0.75 V (**Fig. 2b**), which is necessary to accommodate the underlying faradaic reactions. We also observed some water electrolysis reactions (thus, slightly reduced coulombic efficiency) when the charging/discharging voltage of the symmetric coin cells approached ± 1.25 V and beyond. Therefore, based on the idea of keeping high coulombic efficiency values, it was decided to choose the voltage range of ± 1.20 V, as it provides the best capacity values while containing parasitic reactions. After selecting the voltage range, the effect of the current density on the charge storage capacity was evaluated. **Fig. 2c** clearly shows that the specific capacity of the active material remained fairly constant around 110 mAh g^{-1} regardless of the current density selected when testing the coin cell between 0.32 and 0.02 A g^{-1}. After this analysis, the symmetric cell was subjected to study the cycling stability at 0.16 A g^{-1}. The results displayed in **Fig. 2d** and **Fig. S8** stressed again the high (electro)chemical and dimensional stability (**Fig. S9** and **S10**) of the polymer active-material with almost 100 % coulombic efficiencies, a high discharge capacity of 98.3 mAh g^{-1}, and specific capacity retention of 77 % after 1000 cycles (46 days). Such excellent cycling properties are considered critical for long-term use in practical water desalination systems [58].

The above results pose a clear indication of the superior electrochemical performance demonstrated by the PNDIE for charge storage, even under challenging low electrolyte concentration and dissolved oxygen conditions, in which most of the organic electrode materials fail. These results represent a great prospect for deionization applications.

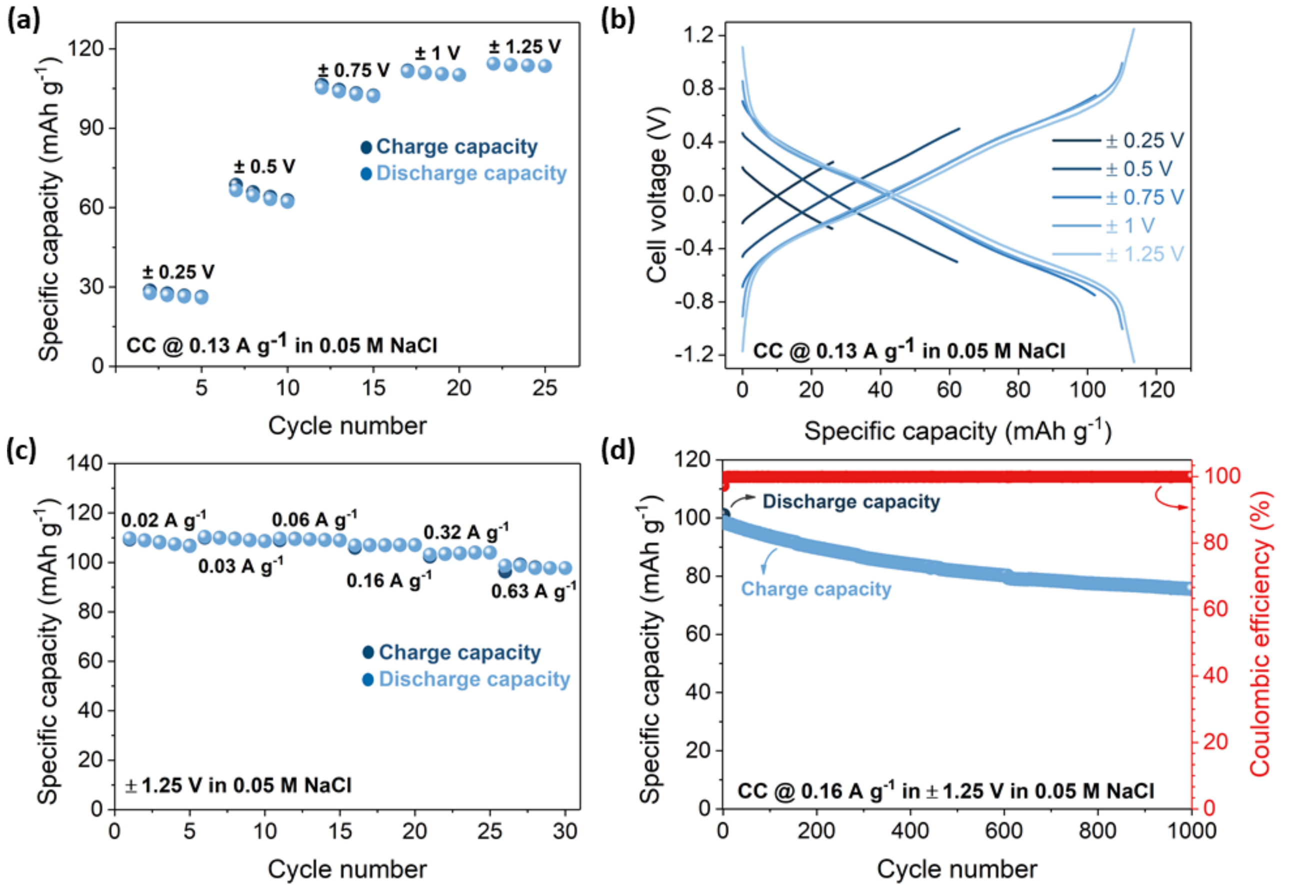

Fig. 2. PNDIE electrochemical performance evaluation in 0.05 M NaCl solution in a symmetric coin cell configuration. Determination of voltage range by GCD at 0.13 A g^{-1}: (a) specific capacity vs. cycle number, and (b) the corresponding GCD profiles. (c) Rate performance, and (d) cycling stability at 0.16 A g^{-1}.

3.3 Electrochemical performance of PNDIE in a FDI symmetric flow cell.

After observing the excellent electrochemical behavior of the PNDIE electrodes, both, in a three-electrode and coin cell configuration, decisive experiments in a real reactor were developed to study the deionization performance. A novel circular flow cell was designed and fabricated by 3D printing looking for maximizing the deionization capacity of the PNDIE self-standing electrodes. The circular form was designed with the aim of homogeneously compressing the electrodes minimizing in this fashion the distance between them, and consequently, reducing the electric resistance.

In this desalination system, the cell architecture consists of two cation-selective faradic electrodes and two parallel flow channels separated by an AEM (**Scheme 1d** and **Fig. S11**). In this configuration, one electrode takes in Na^+ from the feed solution in one flow channel, while the other releases Na^+ into the solution in the opposite channel. At the same time, Cl^- migrates from the Na^+ deficient channel to the Na^+ enriched channel through the AEM, thus generating desalinated and concentrated effluents simultaneously [13]. Once the desalination process is over, the external current is reversed leading to the inversion of the process in each channel. Therefore, by using this configuration, it would be possible in a single pass process to achieve continuous deionization during both steps, charge and discharge, in contrast with the traditional CDI process.

3.3.1 Effect of voltage window

The first set of desalination tests devoted to studying the effect of the voltage window of the full symmetric cell in a constant current mode (0.01 A g^{-1}) was performed with 0.05 M NaCl electrolyte concentration. This is equivalent to a ≈3 g L^{-1}, which is in the range of medium-low salt concentration of brackish waters.

The GCD profiles of the cell voltage shown in **Fig. 3a** depicted the progressive increase of specific capacity (from 20 to 80 mAh g^{-1}) when wider voltage windows were employed (from ± 0.7 to ± 1.2 V, respectively). Furthermore, the good symmetry of the GCD curves in the different voltage windows, suggests good reversibility of the electrode materials during the desalination process, an indication of achieving rapidly the dynamic steady state (DSS) [50,59]. As displayed in **Fig. 3b**, the increase of specific capacity has a good correlation with the variation of conductivity, and thus the difference in the salt concentration detected during the charging step. The results show how the initial conductivity of the effluent corresponding to the positive electrode (PNDIE-Na, which suffers the oxidation) compartment rapidly increased as a consequence of the deintercalation of Na^+. On the other side of the cell, where the PNDIE is located, the conductivity decreased due to the polymer reduction reaction that leads to Na^+ capture.

Note that in this cell configuration, an anion-selective membrane was placed between the electrodes allowing chloride ions to cross from one compartment to the other to compensate for the charge unbalance. Moreover, the membrane provides the separation that prevents the intercalation of cations in the opposite electrode, which would not allow the visualization of the change in the conductivity. The analysis of the conductivity and its conversion to salt concentration difference (Δc) revealed a considerable increase in the deionization capacity associated with the widening of the potential window. This hypothesis was subsequently confirmed by the analysis of the samples by IC (**Table S1**). *SAC* values collected in **Table 1** boosted from 18.0 to 42.1 mg g^{-1} and to 155.4 mg g^{-1} when the window was enlarged from ± 0.7 V to ± 1.0 V and to ± 1.2 V, respectively. We believe that the substantial increase of 8-fold observed in *SAC* values is due to the change from a one single-electron mechanism to a two-electron process. The same effect was previously seen in HCDI processes in which the *SAC* and the charge efficiency were enhanced by applying higher cell voltages [37], allowing the electrode active materials to approach their appropriate redox reaction potentials. This hypothesis is supported by the previous CV and GCD experiments (**Fig. 1 and Fig. 2**) in which the second redox process is observed at lower potentials, especially when the electrolyte solution is more diluted. This effect is expected to become even more important due to the higher contribution of the anionic membrane to the overall resistance of the cell that results in higher overpotential for the faradaic reactions.

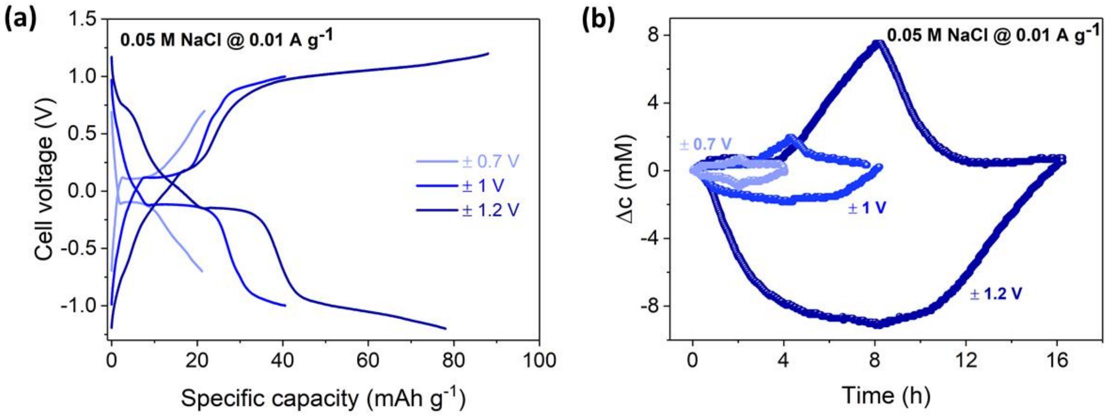

Fig. 3. Optimization of the PNDIE FDI cell's operational voltage window. GCD profiles at 0.01 A g^{-1} performed in 0.05 M NaCl. Comparison of (a) specific capacity and (b) salt concentration difference in each voltage range.

Table 1. Full symmetric FDI cell results (average of three cycles) obtained in 0.05 M NaCl solution at 0.01 A g^{-1} in different voltage windows.

Voltage (V)	Δ*c* (mM)	*SAC* (mg_{NaCl} g_{PNDIE}^{-1})	*ASAR* (mg_{NaCl} g_{PNDIE}^{-1} min^{-1})	*Λ* (%)	E_M (kWh mol^{-1})	E_V (kWh m^{-3})	*P* (L m^{-2} h^{-1})
± 0.7	0.94	18.0	0.15	39	20.9	0.02	16.1
± 1.0	2.22	42.1	0.17	43	27.8	0.06	7.6
± 1.2	8.17	155.4	0.33	83	21.0	0.17	4.0

From the kinetics point of view, *ASAR* values displayed a substantial improvement of more than 50 % (from 0.15 to 0.33 mg g^{-1} min^{-1}) when the potential window was enhanced from ± 0.7 to ± 1.2 V, despite the significant increment of the processing time. Regarding *Λ*, in general, it reflects the disparity between the transferred electrical charge on one hand and salt deficiency or excess in the effluent stream on the other [51]. However, in this case, the PNIDE exhibits a special feature associated with the sodium intercalation mechanism in which, depending on the voltage window, one or two electrons can be transferred. As can be seen in **Table 1**, *Λ* values increased from 39 to 83 % when increasing the voltage clearly showing the impact of shifting from one-electron to two-electron mechanism. The corresponding specific discharge capacity during this desalination process reached ≈86 mAh g^{-1}, which is in the range of values obtained in lab-scale studies, for instance, in the GCD tests in three electrode cell (**Fig. 1e**). This result indicates that the electrochemical capacity of PNDIE is fully utilized when it is assembled in a symmetric system in a ± 1.2 V voltage window being this also in line with the previous report [37].

Finally, operational outputs such as E_M, E_V and, P were calculated. E_M values corroborate the effect of the ion coordination mechanism, showing that, when a higher voltage window is employed, the energy demand is compensated with a higher salt removal. On the other hand, it is expected that P will have a strong impact on capital cost while E_V will have it on operating cost. That means that P and E_V could be used as approximate surrogates for capital and operational costs, respectively [51]. **Table 1** demonstrated that higher voltage windows led to larger Δc, *SAC* and, *ASAR* values although extending the time of solution processing which deeply impacts P. Thus, larger potential windows are associated with longer cycles and lower P. Similarly, widening the cell voltage implies an increment of E_V since the volume of the solution treated in the recirculation mode is the same for all the experiments. Nevertheless, the evaluation of E_V reveals that the energy is being more efficiently used when expanding the operational voltage.

3.3.2 Effect of the current

The desalination performance at different current densities was tested using the largest potential window, ± 1.2 V (**Fig. 4**). As expected, the increase of the current density from 0.01 to 0.04 A g^{-1} led to a proportional reduction of the specific capacity (from 80 to 20 mAh g^{-1}), and the consequent drop of the *SAC* from 155.4 to 102.9 mg g^{-1} (**Table 2**), although still keeping a high desalination capacity. These results are consistent with the GCD characterization performed in the coin cell and have been associated with both, an ineffective ion and/or electron transfer kinetics in the bulk of the electrode, and the electrode potential reduction due to the IR drop [46] at higher current densities.

Despite the *SAC* reduction, as current density increases, the charging/discharging time of the process decreases positively leading to a substantial increment of the *ASAR* from 0.33 to 3.42 mg min^{-1} g^{-1}. An additional benefit of the high current density was the rise in productivity, which boosted from 4 to 62 L h^{-1} m^{-2}. Furthermore, the reduction of the cycle extension has a large influence on E_M and E_V, leading to a significant decline from 21.0 to 5.2 kWh mol^{-1} and 0.17 to 0.03 kWh m^{-3}, respectively, when higher currents were used.

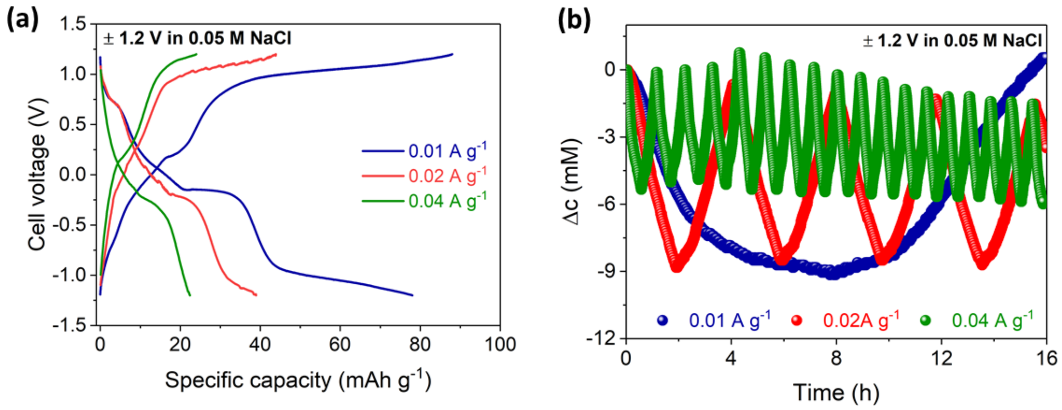

Fig. 4. The average salt adsorption rate evaluation of the PNDIE FDI cell. (a) Galvanostatic charge and discharge profiles for the comparison of the specific capacity and (b) the salt concentration difference at each current density using 30 mL of 0.05 M NaCl solution.

Table 2. Full symmetric cell results (average of three cycles) obtained in 0.05 M NaCl solution in ± 1.2 V at different current densities.

Current density ($\mathbf{A\ g^{-1}}$)	**Δc (mM)**	***SAC* ($\mathbf{mg_{NaCl}\ g_{PNDIE}^{-1}}$)**	***ASAR* ($\mathbf{mg_{NaCl}\ g_{PNDIE}^{-1}\ min^{-1}}$)**	**E_M ($\mathbf{kWh\ mol^{-1}}$)**	**E_V ($\mathbf{kWh\ m^{-3}}$)**	***P* ($\mathbf{L\ h^{-1}\ m^{-2}}$)**
0.01	8.17	155.4	0.33	21.0	0.17	4
0.02	7.52	143.0	1.32	8.8	0.07	17
0.04	5.41	102.9	3.42	5.2	0.03	62

Therefore, the maximum *SAC* in one-half cycle was measured at ~78 mg $\text{g}_{\text{both electrodes}}^{-1}$ for the cell at the lowest current density of 0.01 A g^{-1} being the total salt removed from the feed water was ~155 mg $\text{g}_{\text{both electrodes}}^{-1}$ in one full desalination cycle. These results highlight the benefits of a rocking chair symmetric cell equipped with two identical PNDIE electrodes that can continuously desalinate water in contrast to the asymmetric HCDI systems that require a discharge step leading to a non-continuous desalination process [60].

3.3.3 Effect of the effluent concentration

The system was tested using three different NaCl solution concentrations (0.05 M, 0.03 M, and 0.01 M) setting a potential window of ± 1.2 V at 0.02 A g^{-1}. In this case, the higher the NaCl concentration the larger the desalination capacity, which is coherent with the CV and GCD studies. These results are also consistent with the specific capacity values of desalination experiments (**Fig. S12**). Thus, the reduction of the electrolyte concentration from 0.05 to 0.01 M, led to a capacity drop from 39.4 to 17.1 mAh g^{-1}, and consequently, a contraction of the *SAC* from 155.4 to 30.7 mg_{NaCl}

g_{PNDIE}^{-1} (**Table S2**) and the *ASAR* from 1.32 to 0.60 mg_{NaCl} g_{PNDIE}^{-1} min^{-1}. As mentioned before this behavior was noticed in the CV curves, where the reduction and the oxidation peaks slowly shifts towards the left and right, respectively, indicating that the redox activity of the polyimide is weakened with the decrease of the electrolyte concentration [37]. The larger *SAC* and *ASAR* values observed at higher feed concentrations have been related in the literature with the reduction of resistance component associated with the ionic losses [50,61] and the faster ion transport kinetics, both, in electrolyte and bulk of the buckypaper electrode [59]. This trend has been previously seen with PNDIE in the HCDI cell, in which the SAC gradually increased with the NaCl concentration [37]. Despite this reduction, the *SAC* value obtained at the lowest feed concentration can be considered still very competitive regarding previous results reported in the literature.

In order to have a tentative analysis of the costs of the system and assess the practical viability of these materials (**Fig. S16**) a comparison of the two operational variables, E_V and P is described. Regarding the capital cost, it was observed that P increased with the reduction of the voltage window and the increment of the current density, mainly due to the shorter cycling times used for processing similar volumes. This is consistent with the studies performed by Hawks *et al.*, and Lado *et al.* [9,18,51]. On the other hand, the operational costs (correlated with E_V) boost when either the voltage window or the current density are increased. Despite this increment, E_V values obtained working in the PNDIE system at the highest voltage window (± 1.2 V) and the fastest current density (0.04 A g^{-1}) were found very competitive (0.03 kWh m^{-3} for Δc of 5.4 mM). This is so even when comparing these values with the ones obtained for other symmetric systems, such as a NiHCF cell, that consumed 0.17 kWh m^{-3} for a similar Δc of 5 mM [60].

An additional and similar cost estimation could also be performed using the performance results at different electrolyte concentrations (**Table S2**) to evaluate the energy consumption of a process in which brackish water with an average concentration of 3.0 g L^{-1} (≈ 50 mM) should be reduced to 0.5 g L^{-1} (≈ 8 mM) in order to be discharged. By considering roughly constant *SAC* values between each one of the three different electrolyte concentration levels (50, 30 and 10 mM), and the energy consumption values associated to those inlet concentrations, one could estimate that 0.6-0.7 kWh m^{-3} could be consumed in a multi-step process. Previous publications estimated energy consumption for MCDI to nearly 0.4 kWh m^{-3} when reducing the feed concentration from 34 mM NaCl to 9 mM with an average P of 10 L h^{-1} m^{-2} [62] . Moreover, reported values for brackish water desalination plants operated by reverse osmosis (BWRO) reached 0.5-0.6 kWh m^{-3} for concentration reductions from 5.0 g L^{-1} (86 mM) to 0.5 g L^{-1} (8 mM) [63]. However, a more widen range between 0.6-2.3 kWh m^{-3} has been reported by Pan et al., when analyzing BWRO plants of different capacities [64]. In the case of electrodialysis (ED) the values provided by Ortiz et al. ranged between 0.39-0.85 kWh m^{-3} for a reduction 4.5 g L (76 mM) [65]. Based on the values reported and our estimations, one could conclude that the energy consumption of the all-polymer cell is in the range of more established technologies such as MCDI, RO and ED. Nevertheless, it is important to stress here that the values reported are related to technologies tested at different scales where the range of water production values is quite diverse. Therefore, this comparison should be taken as a first approximation, although confirming that all-polymer faradaic deionization technology has a substantial potential for being used as a brackish water desalination technology.

3.3.4 Cycling stability

Cycling stability is also an important factor to be considered for evaluating the endurance of electrode materials for FDI. A long-term experiment performed using ± 1.0 V voltage window (**Fig. 5**) showed that initially, a conditioning phase occurred during the first 20 cycles in which the capacity increased from 31 to ~73 mAh g^{-1}, which could be related with a membrane activation process. After that phase, the behavior of the PNDIE system stabilized giving a capacity retention of 80 % after 100 cycles. Calculation of the *SAC* over the cycling experiment indicated that values ranged between 24 and 33 mg g^{-1} suffering initially a slight decrease after 20 cycles to finally recover its full capacity (*SAC* retention of 100 %) after 100 cycles (23 days). Subsequently, despite the stability of the discharge capacity over the next 20 cycles, SAC values decreased to 17 mg g^{-1} after 120 cycles. In order to supplement the excellent cycle stability of these practical electrodes, surface morphology characterization by FE-SEM and energy dispersive X-ray spectroscopy (EDS) mapping analyses ware carried out. Both the pristine and post-cycled electrode from the FDI cell reveal similar surface morphologies of randomly oven carbon nanotubes embedding polymer particles without much differences (**Fig. S13**). Additionally, the fraction C, O, N elements by EDS mapping analysis of the pristine (**Fig. S14**) and post-cycled PNDIE electrode (**Fig. S15**) almost remained unchanged. This suggests excellent (electro)chemical stability of PNDIE buckypaper electrodes under practical desalination conditions, despite longevity of the cycling experiment.

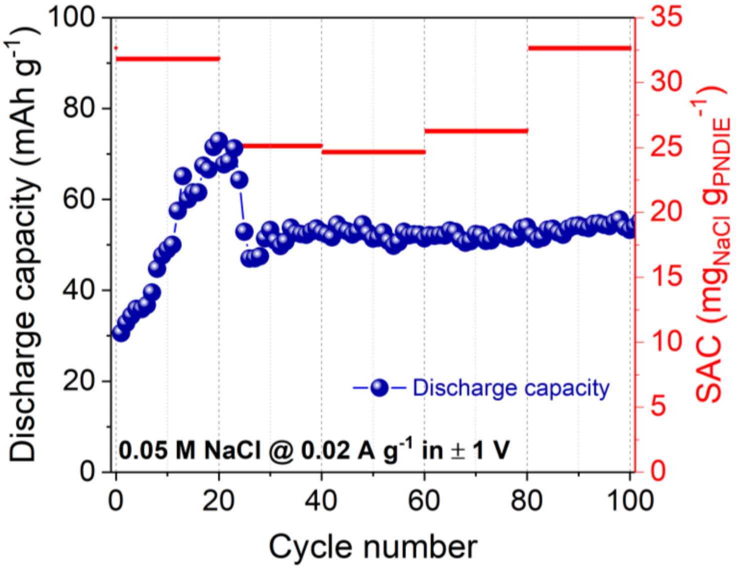

Fig. 5. Cycling performance of the PNDIE FDI cell. CC of 0.02 A g^{-1} in 0.05 M NaCl in ± 1 V and the respective *SAC* obtained taking average values each 20 cycles.

3.3.5 All polymer FDI vs. State-of-the-art

Finally, the performance of the FDI cell constructed by the PNDIE electrodes was compared with the data found in the recent literature about other faradaic electrodes in terms of desalination capacity. As can be observed in **Fig. 6a,** the symmetric PNDIE flow cell reached a maximum *SAC* of 155.4 mg g^{-1} when testing at 0.05 M NaCl, that is, as far as we know, the highest *SAC* value reported in the literature for faradaic electrodes treating brackish water [10,37,58,66–69]. This comparative study was also extended by using the Ragone plot adapted to CDI metrics by Kim and Yoon [70], in which the desalination performance is evaluated taking into consideration both the capacity (*SAC*) and rate (*ASAR*) [70]. The CDI-Ragone plot clearly shows the outstanding performance of the symmetric PNDIE in comparison with reported CDI, HCDI, and FDI systems reaching not only high salt removal capacities but also excellent salt capture rates (**Fig. 6b**). Thus, the lowest and highest tested current intensities provided the best capacity (155.4 mg g^{-1}) and the maximum rate (3.42 mg$_{NaCl}$ g$_{PNDIE}$$^{-1}$ min^{-1}), respectively [70]. The exceptional results obtained with the rocking chair flow cell in a wide range of electrolyte concentrations along with the robust performance observed in the cycling experiments highlight the potential of “All-Polymer” faradaic deionization cells based on PNDIE electrodes for desalination applications.

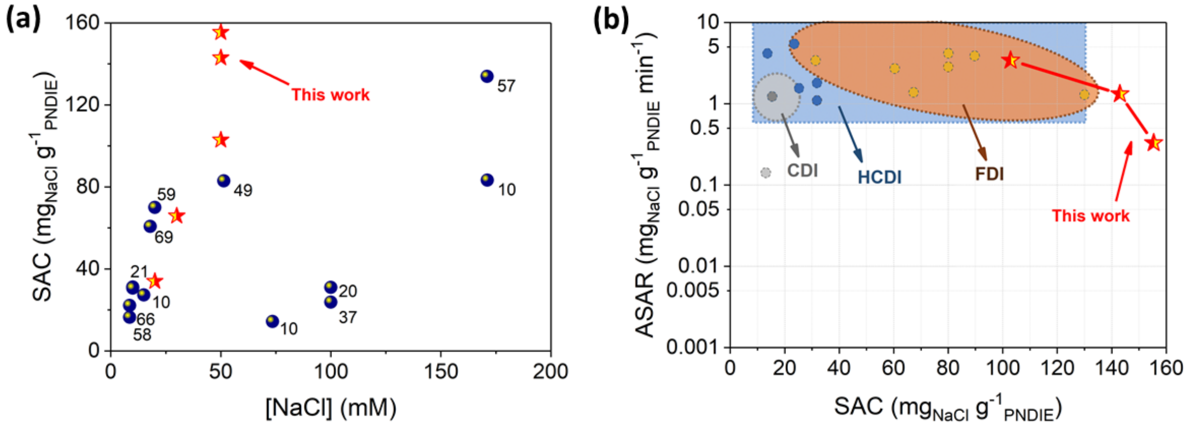

Fig. 6. Comparing PNDIE FDI performance with the state-of-the-art electrochemical deionization literature reports. (a) *SAC* values obtained from literature at different NaCl concentrations (blue dots) including the results obtained in this work (red stars), and (b) Ragone plot. These plots for different electrochemical deionization techniques are computed by considering some of the best performing deionization cells in their class.

4. Conclusion

In this study, the ability of PNDIE to consistently capture and release sodium ions over cycling was exploited for brackish water desalination. First, an innovative methodology based on the preparation of binder- and metal current collector-free buckypaper electrodes using PNDIE, rGO, and SWCNTs was developed to produce practical PNDIE electrodes. Subsequently, the electrochemical performance of the PNDIE electrode was evaluated in a standard three-electrode half-cell and symmetric coin full-cell, revealing promising capacity, cycle stability, and rate capability under challenging low electrolyte concentration (0.05 M) and dissolved oxygen conditions.

After these promising results, a new all-polymer FDI flow cell equipped with practical PNDIE electrodes (mass loading of 9.6 mg cm^{-2}) was designed to produce a desalinated water/brine simultaneously thanks to the rocking chair mechanism. The systematical test of the cell under various operational conditions confirmed the mechanism of the PNDIE cell serving for the first time as a proof-of-concept of this all-polymer symmetric FDI cell. Results indicated that the capacity of Na^+ removal was improved by up to more than 7 times when the voltage window was augmented from ± 0.7 to ± 1.2 V (from 18.0 to 155.4 mg g^{-1}). This exceptional outcome is suggested to be due to a multi-electron redox process of PNDIE that rendered high specific capacity values reflected in the impressive *SAC*, particularly ± 1.2 V. In addition to this, it is important to emphasize that the PNDIE rocking-chair system, besides an ultrahigh desalination capacity, shows also a fast salt removal rate (3.42 mg g^{-1} min^{-1}), and outstanding cycling stability over than 100 cycles (23 days) with a full *SAC* retention. Furthermore, the comparison of these results regarding the state-of-the-art literature reveals the superior performance delivered by all-polymer FDI cell highlighting the relevance of the outcome achieved. As a final conclusion we hypothesize that our approach provides a brief outlook of different experimental analysis that enables to optimize the conditions of the desalination process, paving the way toward the design of advanced and high-performance FDI systems. Overall, the symmetric FDI system composed by simple preparation buckypaper electrodes fabricated using safe and environmentally benign polymers may play a positive role in promoting economical and sustainable electrochemical desalination.

Acknowledgement

NP appreciates fellowship IJC2020-043076-I-I funded by MCIN/AEI/0.13039/501100011033 and by the European Union NextGenerationEU/PRTR. NP and RM acknowledge PID2021-124974OB-C21 financed by MCIN/AEI/10.13039/501100011033/FEDER "A way of making Europe". NG acknowledges the funding from the European Union's Horizon 2020 framework programme under the Marie Skłodowska-Curie agreement No. 101028682. AFP and JJL appreciates the Talento's program of the Community of Madrid which involves the project SELECTVALUE (2020-T1/AMB-19799). The authors also would like to thank Gonzalo Castro and Ignacio Almonacid for collaborating in the laboratory experiments and the sample analysis.

References

[1] E. Bou, EIT InnoEnergy Impact report 2020, 2020. https://sdgs.un.org/es/goals (accessed May 12, 2022).

[2] World Water Assessment Programme (United Nations), UN-Water., Unesco., THE UNITED NATIONS WORLD WATER DEVELOPMENT REPORT 2021, 2021.

[3] Y. Li, Z. Ding, J. Li, K. Wang, T. Lu, L. Pan, Novel membrane-free hybrid capacitive deionization with a radical polymer anode for stable desalination, Desalination. 481 (2020). https://doi.org/10.1016/j.desal.2020.114379.

[4] T.B. Schon, B.T. McAllister, P.F. Li, D.S. Seferos, The rise of organic electrode materials for energy storage, Chem. Soc. Rev. 45 (2016) 6345–6404. https://doi.org/10.1039/c6cs00173d.

[5] B. Zhang, A. Boretti, S. Castelletto, Mxene pseudocapacitive electrode material for capacitive deionization, Chem. Eng. J. 435 (2022) 134959. https://doi.org/10.1016/j.cej.2022.134959.

[6] F. Yu, L. Wang, Y. Wang, X. Shen, Y. Cheng, J. Ma, Faradaic reactions in capacitive deionization for desalination and ion separation, J. Mater. Chem. A. 7 (2019) 15999–16027. https://doi.org/10.1039/c9ta01264h.

[7] E. Jones, M. Qadir, M.T.H. van Vliet, V. Smakhtin, S. mu Kang, The state of desalination and brine production: A global outlook, Sci. Total Environ. 657 (2019) 1343–1356. https://doi.org/10.1016/j.scitotenv.2018.12.076.

[8] E.R. Reale, L. Regenwetter, A. Agrawal, B. Dardón, N. Dicola, S. Sanagala, K.C. Smith, Low porosity, high areal-capacity Prussian blue analogue electrodes enhance salt removal and thermodynamic efficiency in symmetric Faradaic deionization with automated fluid control, Water Res. X. 13 (2021). https://doi.org/10.1016/j.wroa.2021.100116.

[9] J.J. Lado, E. García-Quismondo, I. Almonacid, G. García, G. Castro, J. Palma, A successful transition from a vanadium redox flow battery stack to an energy efficient electrochemical desalination module, J. Environ. Chem. Eng. 9 (2021). https://doi.org/10.1016/j.jece.2021.106875.

[10] H. Yoon, J. Lee, S. Kim, J. Yoon, Review of concepts and applications of electrochemical ion separation (EIONS) process, Sep. Purif. Technol. 215 (2019) 190–207. https://doi.org/10.1016/j.seppur.2018.12.071.

[11] M. Pasta, C.D. Wessells, Y. Cui, F. La Mantia, A desalination battery, Nano Lett. 12 (2012) 839–843. https://doi.org/10.1021/nl203889e.

[12] D. He, C.E. Wong, W. Tang, P. Kovalsky, T. David Waite, Faradaic Reactions in Water Desalination by Batch-Mode Capacitive Deionization, Environ. Sci. Technol. Lett. 3 (2016) 222–226. https://doi.org/10.1021/acs.estlett.6b00124.

[13] Q. Li, Y. Zheng, D. Xiao, T. Or, R. Gao, Z. Li, M. Feng, L. Shui, G. Zhou, X. Wang, Z. Chen, Faradaic Electrodes Open a New Era for Capacitive Deionization, Adv. Sci. 7 (2020). https://doi.org/10.1002/advs.202002213.

[14] J.M.A. Freire, J.J. Lado, E. García-Quismondo, G.C. Burillo, J. Palma, A.R. Loiola, E. Longhinotti, M.A. Anderson, Strategies to boost capacitive deionization performance of 3D electrodes, Sep. Purif. Technol. 273 (2021) 118977. https://doi.org/10.1016/j.seppur.2021.118977.

[15] D. Perez-Antolin, C. Irastorza, S. Gonzalez, R. Moreno, E. García-Quismondo, J. Palma, J.J. Lado, E. Ventosa, Regenerative electrochemical ion pumping cell based on semi-solid electrodes for sustainable Li recovery, Desalination. 533 (2022) 115764. https://doi.org/10.1016/j.desal.2022.115764.

[16] S.D. Datar, R. Mane, N. Jha, Recent progress in materials and architectures for capacitive deionization: A comprehensive review, Water Environ. Res. 94 (2022). https://doi.org/10.1002/wer.10696.

[17] P. Srimuk, J. Lee, A. Tolosa, C. Kim, M. Aslan, V. Presser, Titanium Disulfide: A Promising Low-Dimensional Electrode Material for Sodium Ion Intercalation for Seawater Desalination, Chem. Mater. 29 (2017) 9964–9973. https://doi.org/10.1021/acs.chemmater.7b03363.

[18] J.J. Lado, V. Cartolano, E. García-Quismondo, G. García, I. Almonacid, V. Senatore, V. Naddeo, J. Palma, M.A. Anderson, Performance analysis of a capacitive deionization stack for brackish water desalination, Desalination. 501 (2021). https://doi.org/10.1016/j.desal.2020.114912.

[19] Y. Wang, I. Vázquez-Rodríguez, C. Santos, E. García-Quismondo, J. Palma, M.A. Anderson, J.J. Lado, Graphite felt 3D framework composites as an easy to scale capacitive deionization electrode for brackish water desalination, Chem. Eng. J. 392 (2020) 123698. https://doi.org/10.1016/j.cej.2019.123698.

[20] J. Lee, P. Srimuk, R. Zwingelstein, R.L. Zornitta, J. Choi, C. Kim, V. Presser, Sodium ion removal by hydrated vanadyl phosphate for electrochemical water desalination, J. Mater. Chem. A. 7 (2019) 4175–4184. https://doi.org/10.1039/c8ta10087j.

[21] J. Lee, S. Kim, C. Kim, J. Yoon, Hybrid capacitive deionization to enhance the desalination performance of capacitive techniques, Energy Environ. Sci. 7 (2014) 3683–3689. https://doi.org/10.1039/c4ee02378a.

[22] R. Trócoli, C. Erinmwingbovo, F. La Mantia, Optimized Lithium Recovery from Brines by using an Electrochemical Ion-Pumping Process Based on l-MnO2 and Nickel Hexacyanoferrate, ChemElectroChem. 4 (2017) 143–149.

[23] A. Siekierka, J. Kujawa, W. Kujawski, M. Bryjak, Lithium dedicated adsorbent for the preparation of electrodes useful in the ion pumping method, Sep. Purif. Technol. 194 (2018) 231–238. https://doi.org/10.1016/j.seppur.2017.11.045.

[24] L. Shi, X. Bi, E. Newcomer, D.M. Hall, C.A. Gorski, A. Galal, B.E. Logan, Co-precipitation synthesis control for sodium ion adsorption capacity and cycle life of copper hexacyanoferrate electrodes in battery electrode deionization, Chem. Eng. J. 435 (2022) 135001. https://doi.org/10.1016/j.cej.2022.135001.

[25] S. Porada, A. Shrivastava, P. Bukowska, P.M. Biesheuvel, K.C. Smith, Nickel Hexacyanoferrate Electrodes for Continuous Cation Intercalation Desalination of Brackish Water, Electrochim. Acta. 255 (2017) 369–378. https://doi.org/10.1016/j.electacta.2017.09.137.

[26] S. Kim, J. Lee, C. Kim, J. Yoon, Na2FeP2O7 as a Novel Material for Hybrid Capacitive Deionization, Electrochim. Acta. 203 (2016) 265–271. https://doi.org/10.1016/j.electacta.2016.04.056.

[27] Y. Huang, F. Chen, L. Guo, H.Y. Yang, Ultrahigh performance of a novel electrochemical deionization system based on a NaTi2(PO4)3/rGO nanocomposite, J. Mater. Chem. A. 5 (2017) 18157–18165. https://doi.org/10.1039/c7ta03725b.

[28] T. Chen, L. Xu, S. Wei, Z. Fan, R. Qian, X. Ren, G. Zhou, H. Yang, J. Wu, H. Chen, Ammonia-rich solution production from coal gasification gray water using Chemical-free

Flow-Electrode capacitive deionization coupled with a monovalent cation exchange membrane, Chem. Eng. J. 433 (2022) 133780. https://doi.org/10.1016/j.cej.2021.133780.

[29] J. Lei, Y. Xiong, F. Yu, J. Ma, Flexible self-supporting CoFe-LDH/MXene film as a chloride ions storage electrode in capacitive deionization, Chem. Eng. J. 437 (2022) 135381. https://doi.org/10.1016/j.cej.2022.135381.

[30] H. Oubaha, J.F. Gohy, S. Melinte, Carbonyl-Based π-Conjugated Materials: From Synthesis to Applications in Lithium-Ion Batteries, Chempluschem. 84 (2019) 1179–1214. https://doi.org/10.1002/cplu.201800652.

[31] K.C. Smith, R. Dmello, Na-Ion Desalination (NID) Enabled by Na-Blocking Membranes and Symmetric Na-Intercalation: Porous-Electrode Modeling, J. Electrochem. Soc. 163 (2016) A530–A539. https://doi.org/10.1149/2.0761603jes.

[32] J. Lee, S. Kim, J. Yoon, Rocking Chair Desalination Battery Based on Prussian Blue Electrodes, ACS Omega. 2 (2017) 1653–1659. https://doi.org/10.1021/acsomega.6b00526.

[33] N. Goujon, N. Casado, N. Patil, R. Marcilla, D. Mecerreyes, Organic batteries based on just redox polymers: Abstract, Prog. Polym. Sci. 122 (2021). https://doi.org/10.1016/j.progpolymsci.2021.101449.

[34] P. Poizot, F. Dolhem, J. Gaubicher, Progress in all-organic rechargeable batteries using cationic and anionic configurations: Toward low-cost and greener storage solutions?, Curr. Opin. Electrochem. 9 (2018) 70–80. https://doi.org/10.1016/j.coelec.2018.04.003.

[35] C. Friebe, A. Lex-Balducci, U.S. Schubert, Sustainable Energy Storage: Recent Trends and Developments toward Fully Organic Batteries, ChemSusChem. 12 (2019) 4093–4115. https://doi.org/10.1002/cssc.201901545.

[36] H. Peng, Q. Yu, S. Wang, J. Kim, A.E. Rowan, A.K. Nanjundan, Y. Yamauchi, J. Yu, Molecular Design Strategies for Electrochemical Behavior of Aromatic Carbonyl Compounds in Organic and Aqueous Electrolytes, Adv. Sci. 6 (2019).

https://doi.org/10.1002/advs.201900431.

[37] Y. Li, Z. Ding, J. Li, J. Li, T. Lu, L. Pan, Highly efficient and stable desalination via novel hybrid capacitive deionization with redox-active polyimide cathode, Desalination. 469 (2019). https://doi.org/10.1016/j.desal.2019.114098.

[38] Z. Guo, L. Chen, Y. Wang, C. Wang, Y. Xia, Aqueous lithium-ion batteries using polyimide-activated carbon composites anode and spinel LiMn2O4 cathode, ACS Sustain. Chem. Eng. 5 (2017) 1503–1508. https://doi.org/10.1021/acssuschemeng.6b02127.

[39] T. Gu, M. Zhou, M. Liu, K. Wang, S. Cheng, K. Jiang, A polyimide-MWCNTs composite as high performance anode for aqueous Na-ion batteries, RSC Adv. 6 (2016) 53319–53323. https://doi.org/10.1039/c6ra09075c.

[40] S. Gheytani, Y. Liang, F. Wu, Y. Jing, H. Dong, K.K. Rao, X. Chi, F. Fang, Y. Yao, An Aqueous Ca-Ion Battery, Adv. Sci. 4 (2017) 1–7. https://doi.org/10.1002/advs.201700465.

[41] L. Chen, J.L. Bao, X. Dong, D.G. Truhlar, Y. Wang, C. Wang, Y. Xia, Aqueous Mg-ion battery based on polyimide anode and prussian blue cathode, ACS Energy Lett. 2 (2017) 1115–1121. https://doi.org/10.1021/acsenergylett.7b00040.

[42] Y. Liu, K. Wang, X. Xu, K. Eid, A.M. Abdullah, L. Pan, Y. Yamauchi, Recent Advances in Faradic Electrochemical Deionization: System ArchitecturesversusElectrode Materials, ACS Nano. 15 (2021) 13924–13942. https://doi.org/10.1021/acsnano.1c03417.

[43] T. Liu, K.C. Kim, B. Lee, Z. Chen, S. Noda, S.S. Jang, S.W. Lee, Self-polymerized dopamine as an organic cathode for Li- and Na-ion batteries, Energy Environ. Sci. 10 (2017) 205–215. https://doi.org/10.1039/c6ee02641a.

[44] Z. Ahmad, Aziz, Imani, Abolhassan, Mao, Lijuan, Iqbal, Rashid, Zhang, Hui, Ghazi, Zahid Ali, Ahmad, Rashid, Khan, Adnan Ali, Xie, Lijing, Chen, Cheng-Meng*, Zhang, Zhong and Wei, Adv Materials Technologies - 2019 - Ahmad - A Bifunctional and Free- Standing Organic Composite Film with High Flexibility.pdf, (2019) 1900617.

https://doi.org/10.1002/admt.201900617.

[45] A. Molina, N. Patil, E. Ventosa, M. Liras, J. Palma, R. Marcilla, Electrode engineering of redox-active conjugated microporous polymers for ultra-high areal capacity organic batteries, ACS Energy Lett. 5 (2020) 2945–2953. https://doi.org/10.1021/acsenergylett.0c01577.

[46] G. Hernández, N. Casado, R. Coste, D. Shanmukaraj, L. Rubatat, M. Armand, D. Mecerreyes, Redox-active polyimide-polyether block copolymers as electrode materials for lithium batteries, RSC Adv. 5 (2015) 17096–17103. https://doi.org/10.1039/c4ra15976d.

[47] G. Mohandass, W. Chen, S. Krishnan, T. Kim, Asymmetric and Symmetric Redox Flow Batteries for Energy-Efficient, High-Recovery Water Desalination, Environ. Sci. Technol. 56 (2022) 4477–4488. https://doi.org/10.1021/acs.est.1c08609.

[48] R. Zhao, O. Satpradit, H.H.M. Rijnaarts, P.M. Biesheuvel, A. van der Wal, Optimization of salt adsorption rate in membrane capacitive deionization, Water Res. 47 (2013) 1941–1952. https://doi.org/10.1016/j.watres.2013.01.025.

[49] W. Zhang, X. Wei, X. Zhang, S. Huo, A. Gong, X. Mo, K. Li, Well-dispersed Prussian blue analogues connected with carbon nanotubes for efficient capacitive deionization process, Sep. Purif. Technol. 287 (2022). https://doi.org/10.1016/j.seppur.2022.120483.

[50] M.A. Alkhadra, X. Su, M.E. Suss, H. Tian, E.N. Guyes, A.N. Shocron, K.M. Conforti, J.P. De Souza, N. Kim, M. Tedesco, K. Khoiruddin, I.G. Wenten, J.G. Santiago, T.A. Hatton, M.Z. Bazant, Electrochemical Methods for Water Purification, Ion Separations, and Energy Conversion, Chem. Rev. (2021). https://doi.org/10.1021/acs.chemrev.1c00396.

[51] S.A. Hawks, A. Ramachandran, S. Porada, P.G. Campbell, M.E. Suss, P.M. Biesheuvel, J.G. Santiago, M. Stadermann, Performance metrics for the objective assessment of capacitive deionization systems, Water Res. 152 (2019) 126–137. https://doi.org/10.1016/j.watres.2018.10.074.

[52] N. Patil, A. Aqil, F. Ouhib, S. Admassie, O. Inganäs, C. Jérôme, C. Detrembleur, Bioinspired

Redox-Active Catechol-Bearing Polymers as Ultrarobust Organic Cathodes for Lithium Storage, Adv. Mater. 29 (2017) 1–9. https://doi.org/10.1002/adma.201703373.

[53] Z. Song, H. Zhan, Y. Zhou, Polyimides: Promising energy-storage materials, Angew. Chemie - Int. Ed. 49 (2010) 8444–8448. https://doi.org/10.1002/anie.201002439.

[54] N. Patil, A. Mavrandonakis, C. Jérôme, C. Detrembleur, J. Palma, R. Marcilla, Polymers Bearing Catechol Pendants as Universal Hosts for Aqueous Rechargeable H+, Li-Ion, and Post-Li-ion (Mono-, Di-, and Trivalent) Batteries, ACS Appl. Energy Mater. 2 (2019) 3035–3041. https://doi.org/10.1021/acsaem.9b00443.

[55] M. Jayalakshmi, M.M. Rao, F. Scholz, Electrochemical behavior of solid lithium manganate (LiMn2O4) in aqueous neutral electrolyte solutions, Langmuir. 19 (2003) 8403–8408. https://doi.org/10.1021/la0340448.

[56] L. Chen, W. Li, Z. Guo, Y. Wang, C. Wang, Y. Che, Y. Xia, Aqueous Lithium-Ion Batteries Using O2 Self-Elimination Polyimides Electrodes, J. Electrochem. Soc. 162 (2015) A1972. https://doi.org/10.1149/2.0101510jes.

[57] M.D. Stoller, S.A. Stoller, N. Quarles, J.W. Suk, S. Murali, Y. Zhu, X. Zhu, R.S. Ruoff, Using coin cells for ultracapacitor electrode material testing, J. Appl. Electrochem. 41 (2011) 681–686. https://doi.org/10.1007/s10800-011-0280-5.

[58] W. Shi, X. Liu, T. Deng, S. Huang, M. Ding, X. Miao, C. Zhu, Y. Zhu, W. Liu, F. Wu, C. Gao, S.W. Yang, H.Y. Yang, J. Shen, X. Cao, Enabling Superior Sodium Capture for Efficient Water Desalination by a Tubular Polyaniline Decorated with Prussian Blue Nanocrystals, Adv. Mater. 32 (2020) 1–9. https://doi.org/10.1002/adma.201907404.

[59] G. Zhu, L. Chen, T. Lu, L. Zhang, M.S.A. Hossain, M.A. Amin, Y. Yamauchi, Y. Li, X. Xu, L. Pan, Cu-based MOF-derived architecture with Cu/Cu2O nanospheres anchored on porous carbon nanosheets for efficient capacitive deionization, Environ. Res. 210 (2022). https://doi.org/10.1016/j.envres.2022.112909.

[60] K. Singh, L. Zhang, H. Zuilhof, L.C.P.M. de Smet, Water desalination with nickel hexacyanoferrate electrodes in capacitive deionization: Experiment, model and comparison with carbon, Desalination. 496 (2020). https://doi.org/10.1016/j.desal.2020.114647.

[61] J.J. Lado, R.E. Pérez-Roa, J.J. Wouters, M.I. Tejedor-Tejedor, C. Federspill, M.A. Anderson, Continuous cycling of an asymmetric capacitive deionization system: An evaluation of the electrode performance and stability, J. Environ. Chem. Eng. 3 (2015) 2358–2367. https://doi.org/10.1016/j.jece.2015.08.025.

[62] S. Porada, L. Zhang, J.E. Dykstra, Energy consumption in membrane capacitive deionization and comparison with reverse osmosis, Desalination. 488 (2020) 114383. https://doi.org/10.1016/j.desal.2020.114383.

[63] E. Cabrera, T. Estrela, J. Lora, Pasado, presente y futuro de la desalación en España, Ing. Del Agua. 23 (2019) 199. https://doi.org/10.4995/ia.2019.11597.

[64] S.Y. Pan, A.Z. Haddad, A. Kumar, S.W. Wang, Brackish water desalination using reverse osmosis and capacitive deionization at the water-energy nexus, Water Res. 183 (2020). https://doi.org/10.1016/j.watres.2020.116064.

[65] J.M. Ortiz, J.A. Sotoca, E. Expósito, F. Gallud, V. García-García, V. Montiel, A. Aldaz, Brackish water desalination by electrodialysis: Batch recirculation operation modeling, J. Memb. Sci. 252 (2005) 65–75. https://doi.org/10.1016/j.memsci.2004.11.021.

[66] Z. Zhang, H. Li, Promoting the uptake of chloride ions by ZnCo-Cl layered double hydroxide electrodes for enhanced capacitive deionization, Environ. Sci. Nano. 8 (2021) 1886–1895. https://doi.org/10.1039/d1en00350j.

[67] S. Wang, Z. Li, G. Wang, Y. Wang, Z. Ling, C. Li, Freestanding Ti3C2TxMXene/Prussian Blue Analogues Films with Superior Ion Uptake for Efficient Capacitive Deionization by a Dual Pseudocapacitance Effect, ACS Nano. 16 (2022) 1239–1249. https://doi.org/10.1021/acsnano.1c09036.

[68] Y. Li, Y. Yin, F. Xie, G. Zhao, L. Han, L. Zhang, T. Lu, M.A. Amin, Y. Yamauchi, X. Xu, G. Zhu, L. Pan, Polyaniline coated MOF-derived Mn2O3 nanorods for efficient hybrid capacitive deionization, Environ. Res. 212 (2022) 113331. https://doi.org/10.1016/j.envres.2022.113331.

[69] Z. Liu, H. Li, Exploration of the Exceptional Capacitive Deionization Performance of CoMn2O4 Microspheres Electrode, Energy Environ. Mater. (2021). https://doi.org/10.1002/eem2.12255.

[70] T. Kim, J. Yoon, CDI ragone plot as a functional tool to evaluate desalination performance in capacitive deionization, RSC Adv. 5 (2015) 1456–1461. https://doi.org/10.1039/c4ra11257a.